

Investigation of LiFeAs by means of "Break-junction" Technique

S. A. Kuzmichev^{1,1)}, T. E. Shanygina^{1,2}, I. V. Morozov¹, A. I. Boltalin¹, M. V. Roslova¹, S. Wurmehl³, B. Büchner³

¹*M. V. Lomonosov Moscow State University, 119991 Moscow, Russia*

²*P. N. Lebedev Physical Institute of the RAS, 119991 Moscow, Russia*

³*IFW-Dresden, Institute for Solid State Research, D-01171 Dresden, Germany*

In our tunneling investigation using Andreev superconductor - normal metal - superconductor contacts on LiFeAs single crystals we observed two reproducible independent subharmonic gap structures at dynamic conductance characteristics. From these results, we can derive the energy of the large superconducting gap $\Delta_L = (2.5 \div 3.4)$ meV and the small gap $\Delta_S = (0.9 \div 1)$ meV at $T = 4.2$ K for the $T_C^{local} \approx (10.5 \div 14)$ K (the contact area critical temperature which deviation causes the variation of Δ_L). The BCS-ratio is found to be $2\Delta_L/k_B T_C = (4.6 \div 5.6)$, whereas $2\Delta_S/k_B T_C \ll 3.52$ results from induced superconductivity in the bands with the small gap.

The new class of superconducting rare-earth oxypnictides [1] is still not completely understood and therefore requires further investigation. The layered LiFeAs (111-system) [2] is one of the few stoichiometric Fe-based pnictides which shows neither magnetic nor structural transition but becomes superconducting at 18 K [3, 4]. Band-structure calculations [5, 6, 7] show the Fermi surfaces for 111-system to be comprised of quasi-two-dimensional (2D) hole cylinders centered at the Γ -point and electron ones at the M-point of the first Brillouin zone that can be considered as two effective bands (so called minimal two-band model) [8, 9]. The total density of states at the Fermi level is formed mainly by Fe 3d-states [10, 11, 12, 13, 14]. As was shown in [15], the superconducting transition temperatures T_C for different types of iron-based superconductors correlate with the total density of states at the Fermi level. This fact and the strong Fe isotope effect, which was reported by [16] supports the phonon-mediated coupling importance [17] in these compounds [15, 18]. The electron-phonon coupling is enhanced by an extended van Hove singularity [19] which was shown for iron pnictides and, in particular, for LiFeAs [20]. In this work, we present an investigation of the superconducting properties of LiFeAs single crystals by means of Andreev spectroscopy of superconductor - normal metal - superconductor (SNS) contacts, and the corresponding superconducting gaps.

The LiFeAs single crystals were obtained by self-flux method. The synthesis and investigation of the composition and properties are detailed in [21]. A mixture of small lumps of the Li metal and powders of Fe and As in a molar ratio of Li : Fe : As = 3 : 2 : 3 was

placed into an alumina crucible. All work on the reactive mixture preparation was carried out in a dry box under argon atmosphere. The crucible was inserted into a niobium container, which was welded in argon at 1.5 atm. The sealed Nb container was enclosed in a quartz ampoule. The sample was heated up to 1363 K, kept at this temperature and slowly cooled down to 873 K. At this temperature ampoule was extracted from the furnace and cooled in open air. The LiFeAs single crystals in the form of thin plates with lateral dimensions of $(12 \pm 6) \times (12 \pm 6) \times (0.1 \pm 0.05)$ mm³ were separated from flux mechanically. According to the XRD, EDX, ICP MS, and nuclear quadrupole resonance spectroscopy (NQR) obtained crystals have a stoichiometric composition with a homogeneous distribution of elements over the entire sample [21].

Due to the strong hygroscopicity of LiFeAs, the rectangular plates were kept in glass capillaries. The "break-junction" technique [22, 23] was exploited to make SNS-Andreev contacts. The sample mounting on a spring holder was made in argon atmosphere in order to prevent the material from decomposition in air. The samples (thin plates with dimensions about $(2 \times 1 \times 0.2)$ mm³) were attached to the holder with two current and two potential leads by liquid In-Ga alloy. In order to measure on cryogenically clean surfaces, the holder was bended by a micrometric screw at $T = 4.2$ K causing a microcrack in the sample. The relatively small separation distance between two superconducting banks prevents any extrinsic impurity penetration into the microcrack. The current-voltage curves $I(V)$, their derivatives $dI(V)/dV$ and $R(T)$ -dependences were measured by installation controlled by AT-MIO-16X (National Instruments) digital board [24, 25]. The dynamic con-

¹⁾e-mail: kuzmichev@mig.phys.msu.ru

ductance spectra ($dI(V)/dV$) were obtained following a standard current modulation technique.

Resistive measurements showed the superconducting transition of our $\text{Li}_{1-\delta}\text{FeAs}$ single crystals at T_C^{bulk} ranging from 11 K to 17 K (see Fig.1), which may be caused by a minor affecting of water vapors and leads to a slight variation of lithium amount. As was shown theoretically in [26], while lithium deficiency turns $\text{Li}_{1-\delta}\text{FeAs}$ system into antiferromagnetic state (non superconducting) at $\delta = 0.5$, structure of the Fe-As layers is not changed and c lattice parameter is decreased by $\sim 14\%$ [26]. Obviously, the samples with critical temperature reduced up to $\sim 0.7 T_C^{\text{max}}$ (e.g. filled circles at Fig.1) are described by a small structure deviation from the stoichiometric one. To the best of our knowledge, a variety of physical measurements on the single crystals obtained from the same batch were carried out in [3, 4, 20, 21, 27, 28], see also Table 1 concerning results on T_C and gap values. The samples with the maximal $T_C^{\text{bulk}} \approx 17$ K (see open circles at Fig.1, as well as data published in [21]) demonstrated a relatively narrow superconducting transition (1.2 ÷ 1.5) K, which confirms high quality of single crystals.

To evaluate the superconducting gaps two related methods were used: Andreev spectroscopy [29] of individual superconductor-constriction-superconductor (ScS) [30] Sharvin-type contacts [31] and intrinsic Andreev spectroscopy (intrinsic multiple Andreev reflections effect that usually exists due to steps-and-terraces presence at clean cryogenic clefts). Unlike SN-Andreev contacts, symmetrical ScS-contacts simplify the interpretation of the dynamic conductance spectra by using theoretical model by Kümmel et al. [30]. The main current-voltage characteristic (CVC) features of our ScS-contacts involve an excess current at low voltages and a subharmonic gap structure (SGS), showing series of dips of a dynamic conductance dI/dV at certain bias voltages [30, 32]:

$$V_n = \frac{2\Delta}{en}, \quad n = 1, 2 \dots \quad (1)$$

due to the multiple Andreev reflections effect. In a case of a multi-gap superconductor several independent SGSs corresponding to the each gap should be observable (see Figs.2-5). Such two distinct SGSs were reported earlier at Andreev spectra of $\text{Mg}(\text{Al})\text{B}_2$ break-junctions [33, 34, 35], $\text{LaO}_{0.9}\text{F}_{0.1}\text{FeAs}$ [24], $\text{GdO}(\text{F})\text{FeAs}$ [36, 37, 38], and FeSe [39]. The main advantage of a symmetrical SNS-contact is that at any $T < T_C$ the gap energy can be defined directly from the bias voltages of the peculiarities at the dI/dV -curve making use of the formula (1). The "break-junction" technique

allows one to use such the advantages. The experimental CVCs obtained in this work are typical for the clean classical SNS-contact with excess-current characteristic [30, 32], therefore, the model by Kümmel et al. [30] is valid to describe our data. Strictly speaking, the sharpest SGS usually presents only at $dI(V)/dV$ -characteristic of the most qualitative Andreev contacts with a small diameter a which is less than mean free path of the quasiparticles l (ballistic limit) [31]. In such a case one can observe several gap peculiarities, that increases the accuracy of the gap energies definition. Please note that if $a \approx l$, only the $n = 1$ minima would make a valuable contribution to the dynamic conductance spectra, which was the case for some LiFeAs Andreev contacts studied.

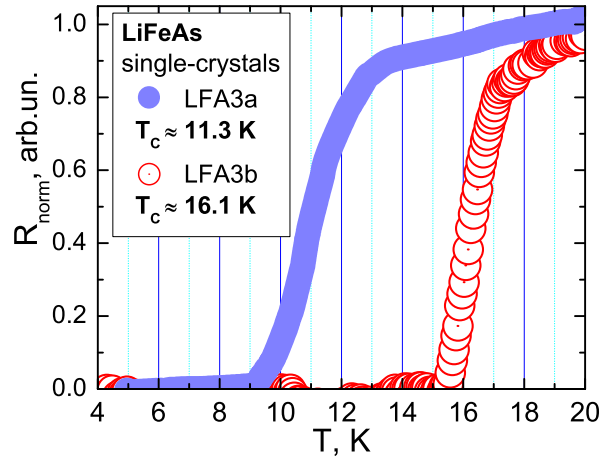


Fig.1. Superconducting transitions for LiFeAs single crystals measured before a microcrack forming. The $dR(T)/dT$ -curve maxima were assigned as T_C^{bulk} . The bulk critical temperatures range from 11 K to 17 K

A significant structure anisotropy of LiFeAs allows us to observe stack contacts [40, 41] representing a sequence of SNS-junctions and intrinsic multiple Andreev reflections effect, which was observed earlier by the "break-junction" technique in other layered superconductors (Bi-2201 [42], $\text{Mg}(\text{Al})\text{B}_2$ [33, 34, 35], and some Fe-based superconductors [24, 39, 38] along the c -direction). The bias voltage at $dI(V)/dV$ -characteristic of such an array scales with the number of contacts N (in a stack) in comparison with dynamic conductance of an individual contact. Existence of natural stacks in c -direction on cryogenic clefts makes usage of such structures typical for "break-junction" technique. The array contacts provide reducing of surface defects influence (which otherwise significantly affect the properties of superconductor [43]) by N times. Therefore, the

magnitude of bulk gaps can be measured with a higher accuracy using stack contacts.

Fig.2 represents the excess-current CVC and the corresponding derivatives for two SNS-Andreev break-junctions (3 contact arrays normalized to a single junction; were formed by a mechanical readjustment) in LiFeAs single crystal measured at $T = 4.2$ K. The main features at the dynamic conductance curve are located at $V_1 = 2\Delta_L/e \approx 5$ mV. The origin of the fine structure is not yet clear and requires further investigation. The observed subharmonic gap structure (SGS) dips $n_L = (1, 2, 3)$ are seemingly related to the large gap (marked by black labels). Peculiarities at $V \approx 3.5$ mV may appear due to an anisotropy of the Δ_L order parameter. However, we need further studies to confirm this unambiguously. The SGS bias voltages described by formula (1) (see inset of the Fig.2) can easily yield the value $\Delta_L \approx 2.5$ meV (at the $T_C^{local} \approx 10.5$ K) without any additional fittings. The "local" T_C is referred to as the T_C measured locally at the contact point with diameter $a \approx l$ and might differ from the T_C obtained by non-local methods. It is worth to note that location of Andreev reflexes were not moved under a mechanical readjustment of the contact while the contact resistance changed (see $I_{7\sim}(V)$ and $I_8(V)$ at Fig.2). Thus, one can conclude that the gap values are still unchanged. This means high homogeneity of the sample superconducting properties in the measuring range.

The dynamic conductance spectra of contacts $\#d5$ and $\#d7$ made on LFA6 sample (see Fig.3) are presented by light and dark-grey curves. Both contacts $\#d5$ and $\#d7$ consist of two SNS-junctions in an array, while contact $\#d7\sim$ (plotted by black dashes) is a stack of three SNS-junctions (all curves are normalized to a single junction). The smearing of the gap peculiarities (Fig.3) presumably originates from the comparatively large contact diameter ($a \approx l$). Another smearing factor might be a temperature influence on the Fermi surface, which scales with $k_B T$: for $T = 4.2$ K it yields an energy uncertainty about 0.4 meV, which is of the same order of magnitude as the value of the small gap (see Fig.4). These are, most likely, the reasons for the fuzzy small gap structure in the case. The complex structure of $n_L = 1$ minima, as well as additional peculiarities in the range of $V_1 \div V_3$ voltages, can be caused by an anisotropy of the Δ_L order parameter. By coinciding the $2\Delta_L$ peculiarities at the stack conductance curves and normalizing them to a single junction (see Fig.3), one can easily yield the large gap energy $\Delta_L \approx 2.5$ meV ($T_C^{local} \approx 10.5$ K). This value corresponds to all the contacts of Fig.3 and does not depend on the contacts resistance changing. Using our gap value, we derive a BCS-

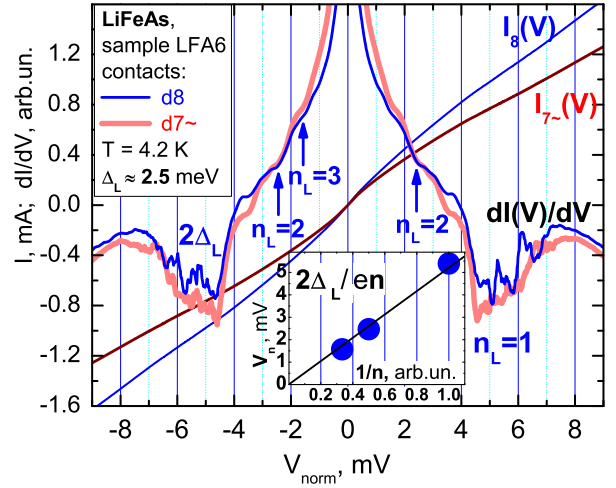


Fig.2. Normalized to a single junction CVC and dynamic conductance of Andreev arrays $\#d7\sim$ (bold light curve) and $\#d8$ (dark thin line) formed by 3 SNS-junctions in a stack ($T = 4.2$ K). The subharmonic gap structure (SGS) minima (n_L labels) define the large superconducting gap $\Delta_L \approx 2.5$ meV which is well-reproduced after the mechanical readjustment of the contact (the $T_C^{local} \approx 10.5$ K). Inset: the linear SGS-minima bias voltages $V_{nL}(1/n)$ -dependence for the aforementioned characteristics

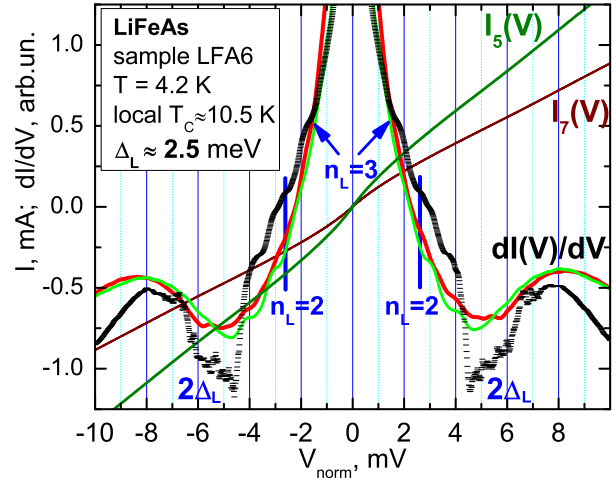


Fig.3. Normalized CVC and dynamic conductance ($T = 4.2$ K) of SNS-Andreev stacks of 2 junctions (contacts $\#d5$, $\#d7$ plotted by light and dark solid lines, respectively) and of 3 junctions (contact $\#d7\sim$, black dashed line). The contacts were formed by a mechanical readjustment. The well-reproduced minima (n_L labels) define the $\Delta_L \approx 2.5$ meV (the $T_C^{local} \approx 10.5$ K)

ratio for LiFeAs $2\Delta_L/k_B T_C \approx 5.5$. In an attempt to consider those conductance spectra as 4 contacts ($\#d5$, $\#d7$) and 6 contacts ($\#d7\sim$) in an array, one could get

$2\Delta_L/k_B T_C \approx 2.8$ for the large gap that is inconsistent with the BCS coupling limit of 3.52.

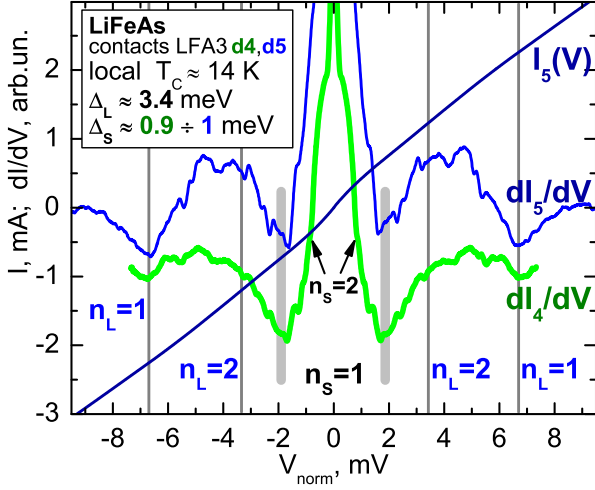


Fig.4. Normalized to a single junction CVC and dynamic conductance ($T = 4.2$ K) of #d4 (light curve) and #d5 (dark curve) Andreev arrays (2 SNS-junctions in stacks). Two sets of Andreev minima ($n_{L,S}$ labels) define the large gap $\Delta_L \approx 3.4$ meV (the $T_C^{local} \approx 14$ K) and the small gap $\Delta_S = 0.9 \div 1.0$ meV. Linear background was suppressed

The SNS-Andreev spectra of stack contacts with the maximal $T_C^{local} \approx 14$ K are shown at Fig. 4. The arrays representing two-contact stacks were formed by sequent junction readjustment. The CVC and the dynamic conductance comprising two sets of Andreev peculiarities in agreement with the formula (1) yield the values $\Delta_L \approx 3.4$ meV and $\Delta_S \approx 0.9$ meV (contact #d4), $\Delta_S \approx 1$ meV (contact #d5). For the contact #d5, the $n_S = 1$ peculiarity was taken as the center of the doublet. Such a structure may be caused by a s-wave symmetry distortion of Δ_S due to the complex form of the hole-like Fermi surface sheets. The reproducibility of the small gap minima ($n_S = 1$) at $dI(V)/dV$ -characteristics of Andreev stacks confirms the existence of the small superconducting gap and suggests it to be a bulk property of LiFeAs. The results presented at Figs.2,3 allow the same conclusion for the large gap. The minima $n_S = 2$ for the small gap become observable on subtracting a straight line at the $dI(V)/dV$ raise region near zero bias.

The temperature affecting on Andreev peculiarities is shown at Fig.5a. The $T_C^{local} \approx 12.5$ K is obtained from the linearization of the CVC derivative. The dynamic conductance dips series (black labels) seemingly reveal the superconducting gap $\Delta \approx 2.5$ meV. It is easy to observe that Δ -minima marked as $n_L = 1$ start to close at $T \approx 6$ K. The gap temperature dependence

$\Delta(T)$ (being in fact the $V_1/2$ positions plotted versus T) is presented at the Fig.5a inset. The aforementioned $T \approx 6$ K appears to be approximately a half of the T_C^{local} . The $\Delta(T)$ was fitted by the single-band BCS-like curve and the two-band dependence (plotted in a framework of Moskalenko [44] and Suhl [45] equations for a superconductor with $\Delta_L/\Delta_S \approx 3.5$ and a weak interband coupling). Both the theoretical curves tend to the $T_C^{local} = 12.5$ K, in the same time, the best fitting is achieved if the two-band curve approaching $T = 0$ K lies above the single-band one. This gives the average gap value about 2.5 meV. The fitting curves behavior indicates no evidence for an induced superconductivity in the condensate under consideration. Hence, this gap parameter is related to the bands with the large, “driving” gap Δ_L and relevant neither to small gap, nor to a surface gap.

The comparable temperature dependences of the large gap $\Delta_L(T)$ for the contacts #d5, LFA3 sample (see the dark curve at Fig.4) and #c, LFA5 sample are shown at Fig.5b. The experimental points were fitted by single-gap BCS-type functions. The reproducibility of the large gap behavior is obvious. Despite the difference in the Δ_L and T_C^{local} values for the contacts, the corresponding BCS-ratios $2\Delta_L/k_B T_C$ are close to each other and approximately equal to 5.6. The closer examination brings out the $\Delta_L(T)$ deviations from the BCS-like curves: all the experimental dependences slightly bend, which originates from nonzero interband interaction with Δ_S -bands. As for the $\Delta_S(T)$ temperature dependence represented by small circles at Fig.5b (contact #d5, LFA3 sample), its behavior is typical for a “driven” gap. The similar phenomenon was observed in Mg(Al)B₂ superconductor earlier [34, 35]. The difference between $\Delta_L(T)$ and $\Delta_S(T)$ courses becomes another evidence for existence of two nearly independent superconducting condensates described by the two gap values in LiFeAs.

There are no published tunneling data (energetic parameters obtained with a help of SIS-, NS-, NIS-, SNS-spectroscopies) on LiFeAs so far. It was revealed in the present work for the first time. Therefore, we compare our results with the data by the number of scientific groups in the Table 1. Angle-resolved photoemission spectroscopy (ARPES) on LiFeAs single crystals [3, 27, 28], specific heat [27, 46], London penetration depth [28, 47, 48], and microwave surface impedance [49] yield similar results for the number and values of superconducting gaps (see Table 1). The distinction in the BCS-ratio values should be taken into account. On calculating $2\Delta/k_B T_C$ the T_C^{onset} in [3, 27, 28, 46, 47, 49, 50] and T_C^{bulk} in [48] have been used, which are average

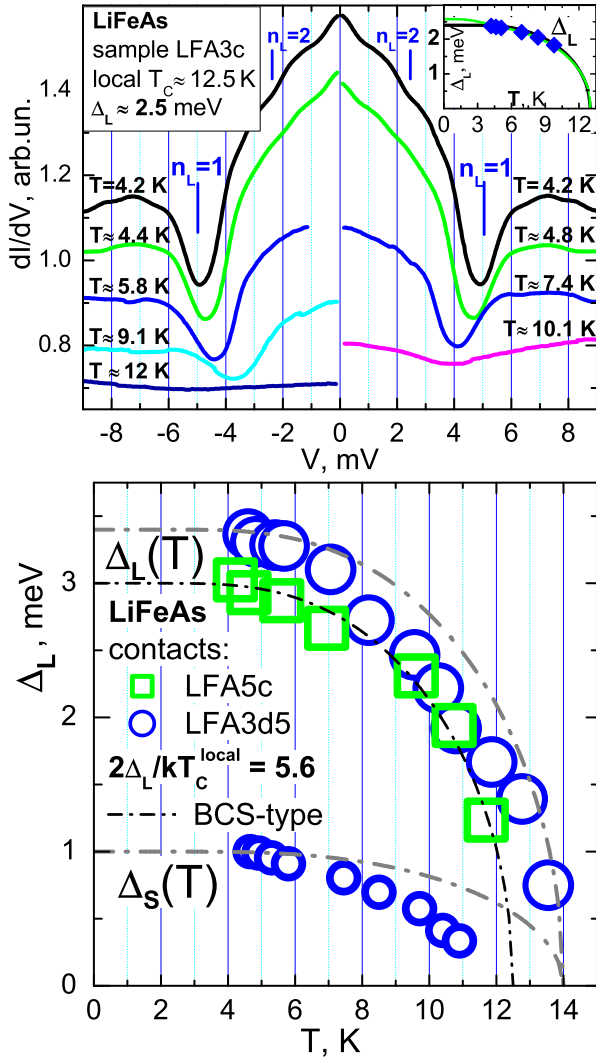


Fig.5. a) Dynamic conductance of LiFeAs Andreev single SGS junction measured at the temperatures ranging from 4.2 K to $T_C^{local} \approx 12.5$ K. SGS defines the large gap $\Delta_L \approx 2.5$ meV (n_L labels). The curves were shifted along the vertical scale for the sake of clarity. Inset: The large gap temperature dependence plotted using experimental data of Fig.5 (rhombus). The single-band BCS-like fit (dark line) and possible two-band fit (light line) were presented. b) The comparison of the large gap temperature dependences: sample LFA5, contact #c (squares; $T_C^{local} = 12.5 \pm 1$ K, $\Delta_L(4.2 \text{ K}) \approx 3$ meV), and sample LFA3, contact #d5 (circles; $T_C^{local} = 14 \pm 1$ K, $\Delta_L(4.2 \text{ K}) \approx 3.4$ meV, $\Delta_S(4.2 \text{ K}) \approx 1$ meV; see Fig. 4). The point size reflects a gap value uncertainty. The single-band BCS-like dependences are plotted by dash-dotted lines

values that may be higher or lower than the T_C^{local} in the point of gap defining due to a samples inhomogeneity if any. By contrast, operating with the local T_C , one can calculate the BCS-ratio value more accu-

ately. For the reason given above our BCS-ratio value exceeds that of other groups obtained by other methods. Nevertheless, an excellent correspondence is revealed with the $2\Delta_L/k_B T_C$ value from [50] (see Table 1). For the large gap, our experimental data lead to ratio $2\Delta_L/k_B T_C = (4.6 \div 5.6)$ which exceeds the standard one 3.52 for single-gap BCS superconductors in the weak coupling limit. At the same time, the BCS-ratio for the small gap $2\Delta_S/k_B T_C \ll 3.52$ indicates the superconductivity induced by interband coupling with the "driving" bands (characterized by the large gap Δ_L) in the bands with Δ_S due to k-space (internal) proximity effect [51] between two condensates, which resembles the situation in $\text{Mg}(\text{Al})\text{B}_2$ [33, 34, 35], and some Fe-based superconductors [24, 36, 37, 38, 39].

In conclusion, it was found that $I(V)$ and $dI(V)/dV$ -characteristic of the SNS-Andreev break-junctions in LiFeAs single crystals with bulk critical temperature $= (11 \div 17)$ K could not be described in a framework of the standard single-gap model. Being observed by Andreev spectroscopy on LiFeAs for the first time, two independent subharmonic gap structures indicating the existence of multi-gap superconductivity yield the following energies of two distinct superconducting gaps: $\Delta_L = (2.5 \div 3.4)$ meV and $\Delta_S = (0.9 \div 1)$ meV (at $T = 4.2$ K and the $T_C^{local} \approx (10.5 \div 14)$ K). The uncertainty in the determination of the gap can be estimated to be about 10% for large gap Δ_L and 20% for Δ_S owing to enormous raise of dynamical conductance at low bias voltages. The estimated BCS-ratios $2\Delta_L/k_B T_C = (4.6 \div 5.6)$ exceeding the single-gap weak-coupling limit 3.52 can be caused by a strong coupling in the "driving" electron-bands [3] characterized by the large gap. On the other hand, the ratio for the small gap $2\Delta_S/k_B T_C \ll 3.52$ hints on the importance of interband coupling (due to k-space proximity effect) that is to be taken into account when considering superconducting properties of LiFeAs.

The authors are grateful to Prof. Ya.G. Ponomarev for providing techniques and materials. We also thank S.V. Borisenko, A.N. Vasiliev and V.M. Pudalov for helpful discussions. This work was supported by the Russian Ministry of Education and Science (projects 11.519.11.6012, MK-3264.2012.2) and by the Russian Foundation for Basic Research (projects 12-03-91674-ERA_a, 12-03-01143-a). Funding by the German research society DFG in project BE1749/13 is gratefully acknowledged.

1. Y. Kamihara, et al., J. Am. Chem. Soc. **128**, 10012 (2006); *ibid.* **130**, 3296 (2008).

2. X.C. Wang, et al., Sol. St. Comm. **148**, 538 (2008); J.H. Tapp, et al., Phys. Rev. B **78** 060505(R) (2008).
3. S.V. Borisenko, et al., Phys. Rev. Lett. **105**, 067002 (2010).
4. O. Heyer, et al., Phys. Rev. B **84** 064512 (2011).
5. D.J. Singh, and M.-H. Du, Phys. Rev. Lett. **100**, 237003 (2008); D.J. Singh, Physica C **469**, 418 (2009)
6. I.A. Nekrasov, et al., JETP Lett. **88**, 144 (2008).
7. A.I. Coldea, et al., Phys. Rev. Lett. **101**, 216402 (2008).
8. S. Raghu, et al., Phys. Rev. B **77**, 220503(R) (2008).
9. J. Li, Y.-P. Wang, Chin. Phys. Lett. **25**, 2232 (2008).
10. E.Z. Kurmaev, et al., J. Phys.: Cond. Matt. **21**, 345701 (2009).
11. T. Miyake, et al., J. Phys. Soc. Jpn. **79**, 044705 (2010).
12. C. Platt, et al., Phys. Rev. B **84**, 235121 (2011).
13. R.A. Jishi, H. M. Alyahyaie, Adv. Cond. Mat. Phys. **2010**, 804343 (2010).
14. I.A. Nekrasov, et al., JETP Letters **88**, 543 (2008).
15. E.Z. Kuchinskii, et al., JETP Lett. **91**, 518 (2010).
16. R. H. Liu, et al., Nature **459**, 64 (2009).
17. J. Bardeen, et al., Phys. Rev. **108**, 1175 (1957).
18. L. Boeri, et al., Physica C **469**, 628 (2009).
19. A.A. Abrikosov, Physica C **317-318**, 154 (1999).
20. A.A. Kordyuk, et al., Phys. Rev. B **83**, 134513 (2011).
21. I. Morozov, et al., Cryst. Growth & Design **10**, 4428 (2010).
22. J. Moreland, J.W. Ekin, J. Appl. Phys. **58**, 3888 (1985).
23. J. Müller, et al., Physica C **191**, 485 (1992).
24. Ya.G. Ponomarev, et al., Phys. Rev. B **79**, 224517 (2009).
25. Ya.G. Ponomarev, A.V. Rakhmanina, Prib. Tehn. Eksp. **5**, 120 (1970).
26. I.R. Shein, A.L. Ivanovskii, Pis'ma v ZhETF **88**, 377 (2008).
27. U. Stockert, et al., Phys. Rev. B **83**, 224512 (2011).
28. D.S. Inosov, et al., Phys. Rev. Lett. **104**, 187001 (2010).
29. A.F. Andreev, Soviet Phys. JETP **19**, 1228 (1964).
30. R. Kümmel et al., Phys. Rev. B **42**, 3992 (1990).
31. Yu.V. Sharvin, Zh. Eksp. Teor. Fiz. **48**, 984 (1965).
32. B.A. Aminov, et al., Phys. Rev. B **53**, 365 (1996).
33. Ya.G. Ponomarev, et al., Sol. St. Comm. **129**, 85 (2004).
34. Ya.G. Ponomarev, et al., JETP Lett. **79**, 484 (2004).
35. S.A. Kuzmichev, et al., Sol. St. Comm. **152**, 119 (2012).
36. T.E. Shanygina, et al., JETP Letters **93**, 94 (2011).
37. V.M. Pudalov, et al., UFN **181**, 672 (2011).
38. T.E. Shanygina, et al., submitted to J. Phys.: Conf. Ser. (2012).
39. Ya.G. Ponomarev, et al., JETP **140**, 527 (2011).
40. H. Nakamura, et al., Phys. Soc. Jpn. **78**, 123712 (2009).
41. T. Matsui, et al., Jap. J. Appl. Phys. **25**, L671 (1986).
42. Ya.G. Ponomarev, et al., Inst. Phys. Conf. Ser. **167**, 241 (2000).
43. E. Heumen, et al., Phys. Rev. Lett. **106**, 027002 (2011).
44. V.A. Moskalenko, Phys. Met. Metall. **4**, 503 (1959).
45. H. Suhl, et al. Phys. Rev. Lett. **12**, 552 (1959).
46. F. Wei, et al., Phys. Rev. B **81**, 134527 (2010).
47. Y.J. Song, et al., Europhys. Lett. **94**, 57008 (2011).
48. H. Kim, et al., Phys. Rev. B **83**, 100502(R) (2011).
49. Y. Imai, et al., J. Phys. Soc. Jpn. **80**, 013704 (2011).
50. K. Sasmal, et al., Phys. Rev. B **81**, 144512 (2010).
51. I.K. Yanson, et al., Phys. Rev. B **67**, 024517 (2003).

Table 1. Comparison of LiFeAs experimental data obtained by different techniques. *The mean T_C defined from the $dR(T)/dT$ derivative was used. **The data range reflects an anisotropy of Δ_S order parameter [3].

<i>Present data (SNS break-junction)</i>						
Sample	Contact	T_C^{local} , K	Δ_L , meV	Δ_S , meV	$2\Delta_L/k_B T_C$	$2\Delta_S/k_B T_C$
LFA6	$d5, d7, d7^\sim, d8$	10.5 ± 0.5	≈ 2.5	-	5.5	-
LFA3b	c	12.5 ± 0.5	≈ 2.5	-	4.6	-
LFA3b	$d4$	14 ± 0.5	≈ 3.4	≈ 0.9	5.6	1.5
LFA3b	$d5$	14 ± 0.5	≈ 3.4	≈ 1	5.6	1.6
<i>Experimental data obtained on the single crystals from the same batch (as samples used by us)</i>						
Ref.	Technique	T_C^{onset} , K	Δ_L , meV	Δ_S , meV	$2\Delta_L/k_B T_C$	$2\Delta_S/k_B T_C$
Borisenko, et al. [3]	ARPES	18	3.2	$1.5 \div 2.5^{**}$	≈ 4.1	$1.9 \div 3.2$
Stockert, et al. [27]	specific heat, ARPES	17	2.6	1.2	≈ 3.5	≈ 1.7
Inosov, et al. [28]	London penetration depth, ARPES	17	3.1	-	4.1	-
<i>Experimental data published by other scientific groups</i>						
Wei, et al. [46]	specific heat	17	2.7 ± 0.8	0.5 ± 0.2	3.5	1.2
Song, et al. [47]	London penetration depth	17.5	2.9	≈ 1.3	≈ 3.8	≈ 1.7
Kim, et al. [48]	London penetration depth	$\approx 17^*$	≈ 2.8	≈ 1.6	≈ 3.8	≈ 2.2
Imai, et al. [49]	microwave surface impedance	17	2.9	-	4.0	-
		16.3	3.0	1.1	4.2	≈ 1.6
		15.6	3.0	1.65	4.4	≈ 2.5
Sasmal, et al. [50]	vortex penetration, reversible magnetization	$14 \div 15.3$	3.3	0.6	5.4	1